Feature Space Clustering for Trabecular Bone Segmentation

Benjamin Klintström[1,2(✉)], Eva Klintström[1,3], Örjan Smedby[1,2,3], and Rodrigo Moreno[2]

[1] Center for Medical Image Science and Visualization, Linköping University, Linköping, Sweden
Benklint@gmail.com
[2] KTH Royal Institute of Technology, School of Technology and Health, Huddinge, Stockholm, Sweden
[3] Department of Medical and Health Science, Division of Radiology, Linköping University, Linköping, Sweden

Abstract. Trabecular bone structure has been shown to impact bone strength and fracture risk. *In vitro*, this structure can be measured by micro-computed tomography (micro-CT). For clinical use, it would be valuable if multi-slice computed tomography (MSCT) could be used to analyse trabecular bone structure. One important step in the analysis is image volume segmentation. Previous segmentation techniques have either been computer resource intensive or produced sub-optimal results when used on MSCT data. This paper proposes a new segmentation method that tries to balance good results against computational complexity.

Material. Fourteen human radius specimens where scanned with MSCT and segmented using the proposed method as well as two segmentation methods previously used to segment trabecular bone (Otsu and Automated Region Growing (ARG)). The proposed method (named FCH) uses a combination of feature space clustering, edge detection and hysteresis thresholding. For evaluation, we computed correlations with the reference method micro-CT for 7 structure parameters and measured segmentation time.

Results. Correlations with micro-CT were highest for FCH in 3 cases, highest for ARG in 3 cases, and in general lower for Otsu. Both FCH and ARG had correlations higher than 0.80 for all parameters, except for trabecular thickness and trabecular termini. FCH was 60 times slower than Otsu, but 5 times faster than ARG.

Discussion. The high correlations with micro-CT suggest that with a suitable segmentation method it might be possible to analyse trabecular bone structure using MSCT-machines. The proposed segmentation method may represent a useful balance between speed and accuracy.

Keywords: Feature-space · Clustering · Segmentation · Trabecular bone

1 Introduction

Besides overall bone mass, the structure of the trabecular bone network has been shown to greatly influence bone strength and the risk of fractures [1–3]. Skeletal structures that mainly consist of trabecular bone are the vertebrae and they are also commonly affected by fractures among the elderly [4].

P. Sharma and F.M. Bianchi (Eds.): SCIA 2017, Part II, LNCS 10270, pp. 65–75, 2017.
DOI: 10.1007/978-3-319-59129-2_6

In vitro, trabecular bone structure can be measured by micro-computed tomography (micro-CT) and by histomorphometry of bone biopsies and these two methods show good agreement [5]. *In vivo,* trabecular bone structure can be measured by high-resolution peripheral quantitative CT (HR-pQCT) [6]. Another clinically available device that shows promise for trabecular structure analysis is cone-beam computed tomography (CBCT), for which *in vitro* studies show good agreement to micro-CT data [7]. The method for imaging the vertebrae in clinical practise is multi-slice computed tomography (MSCT). Previous studies on MSCT have shown good agreement with micro-CT regarding parameters like bone volume over total volume (BV/TV), while other parameters like trabecular nodes (Tb.Nd) and trabecular separation (Tb.Sp) have not been as strongly correlated [8, 9]. Due to its clinical use for imaging the vertebrae, it would be interesting if data from MSCT machines could be used to measure trabecular bone structures parameters.

One important step in calculating trabecular bone structure parameters is the segmentation algorithm used to separate bone from other tissues in the imaged volume [10]. Segmentation can be performed in different ways. For example, an automatic or manual intensity threshold can be effective for high resolution images. Segmenting images acquired with HR-pQCT, CBCT and MSCT is more challenging. Our group has previously shown good results for segmenting CBCT data by using the automated region growing method (ARG) proposed in [11]. There are also segmentation methods using clustering-algorithms [12], but, to the best of our knowledge, they have not been applied for segmenting trabecular bone so far.

The aim of this paper is to suggest a new way of segmenting trabecular bone images using a combination of edge-detection, clustering and thresholding as well as to investigate the possibility of using MSCT data to measure trabecular bone structure parameters.

2 Materials and Methods

2.1 Material

Fourteen human radius specimens from cadavers were used for the analysis. The radius specimens were donated for medical research in accordance with the ethical guidelines regulating such donations at the University of California, San Francisco. The specimens have been used in previous studies from our group [13–16]. The specimens are almost cubic with a side of 12–15 mm and they all include a slab of cortical bone, facilitating orientation.

2.2 Image Acquisition

The images were acquired using two machines:

- One Multi-Slice Computed Tomography, the Somatom Force (Siemens AG, Erlangen Germany). The acquisition was performed using the protocol for imaging the middle ear bones with a tube voltage of 120 kVp and a tube current 230 mAs.

The slice thickness was 400 μm, the increment between slices 200 μm, the pitch 0.8 and the FOV 50 mm, resulting in an intra-slice-resolution of 98 × 98 μm. This machine will be referred to as MSCT.

- One Micro-Computed Tomography, the Skyscan 1176 (Bruker micro-CT, Kontich Belgium). The images were acquired using a tube voltage of 65 kV and a tube current of 385 μA. The total exposure time was approximately 2 h. The resulting volumes had an isotropic resolution of 8.67 μm. This machine will be referred to as micro-CT.

The comparisons were made with the micro-CT data segmented using Otsu-thresholding as a gold standard [17]. The MSCT data were interpolated to an isotropic resolution of 98 μm using spline-interpolation in MATLAB (Mathworks).

2.3 Specimen Preparation and Imaging

Before imaging, the bone samples were de-fatted and then placed in test tubes filled with water. During imaging with the MSCT the test tubes were then placed in the centre of a paraffin cylinder with a diameter of 100 mm. To simulate measurements *in vivo*, a paraffin cylinder was used to simulate soft tissue.

2.4 Image Pre-processing

After imaging and interpolation, the MSCT-volumes were manually registered using the micro-CT volumes as references to ensure as close a match as possible between the processed Volumes of Interests (VOI:s). This registration was performed in two steps using the manual registration tools in MeVisLab (MeVis Medical Solutions AG). This resulted in digitally extracted cubes consisting only of trabecular bones with sides of approximately 8 mm.

2.5 Image Segmentation Using Feature-Space Clustering

The proposed segmentation uses a combination of feature-space clustering with k-means and hysteresis thresholding [18, 19].

This algorithm starts with a pre-filtering step to reduce noise in the data and produce a smoother final segmentation. First with a median filter with a kernel size of approximately twice the mean thickness of trabecular bone, which has been determined from the micro-CT-data, and then with a Gaussian filter with a standard deviation equal to the thickness of trabecular bone.

To facilitate later calculations, the grayscale is then normalized to be centred at 0 with a fixed standard deviation. For this algorithm the standard deviation was set to 500 as previous testing from our group has found that it approximately equals the average for multiple different types of CT-machines (CBCT, HR-pQCT and MSCT). However, the exact value chosen has limited impact on the final segmentation. The intensity values after this pre-processing will be referred to as α.

The next step in the algorithm is to use a combination of Canny and Sobel edge detection in 3D to find the edges of the trabecular structure as well as the direction and magnitude of those edges [20, 21]. The information on the edges was then used to give each voxel a value based on whether it was inside or outside of the edges as well as the magnitude of the edges around it, voxels inside of a strong edge were assigned a large positive value and voxels outside of a strong edge were instead assigned a large negative value. Voxels inside or outside of weak edges were instead assigned a smaller positive or negative value and the values assigned by this function were stored in a matrix. These values will later be referred to as β. Notice that this idea is somehow similar to level sets where a signed distance transform is defined and the edges are defined as zero crossings of such a function. The main advantage of using Canny and Sobel is that the computational complexity is largely reduced compared to level sets.

The next part of the algorithm performs a local normalization of α and β. The average of the six-neighbours and their six-neighbours of every voxel is subtracted from its original intensity value α and β independently. The normalized images are referred to as δ and γ, respectively for α and β. This normalization procedure is performed in order to improve the performance of the method on regions with locally varying grayscales, which is typical in trabecular bone.

At this stage a four-dimensional feature space is created, where each voxel gets its position based on the α-, β-, δ- and γ-values assigned to it. After this, k-means is used in order to split that feature space into two clusters, which should correspond to bone and background. The centre of these two clusters is then used to calculate the Euclidian distance d of each voxel p from those centres in the feature-space:

$$d_{(\mathrm{P,C})} = \sqrt[2]{(\alpha_\mathrm{p} - \alpha_\mathrm{c})^2 + (\beta_\mathrm{p} - \beta_\mathrm{c})^2 + (\delta_\mathrm{p} - \delta_\mathrm{c})^2 + (\gamma_\mathrm{p} - \gamma_\mathrm{c})^2} \tag{1}$$

where c is the centre of the cluster.

The cluster whose centre has the lower α value is assumed to represent the background (in our case water) and the one with the higher α value the foreground (which should be trabecular bone). Each voxel is then assigned the value of the quotient λ(p) between the distance from the centre of the background cluster and the distance from the centre of the bone cluster:

$$\lambda_{(\mathrm{p})} = \frac{d_{(\mathrm{p},\mathrm{c}_\mathrm{background})}}{d_{(\mathrm{p},\mathrm{c}_\mathrm{bone})}} \tag{2}$$

where $\mathrm{c}_\mathrm{background}$ and, c_bone are the two cluster centres.

After λ has been calculated, hysteresis thresholding is applied to λ in 3D. First, an upper threshold is used to segment the image, and the voxels exceeding this threshold are assigned a value of 1 while zero is assigned to the remaining voxel. The voxel is also segmented using a lower threshold. The segmentation using the upper threshold is then iteratively expanded into its six-neighbourhood. Voxels not belonging to the lowest segmentation are filtered out. This procedure is then repeated with the resulting matrix until the result no longer changes between two iterations. Figure 1 shows the

```
Function hysteresis
new = λ >5;
low = λ >0.9;
old = low;

while new != old
    old = new;
    new = dilate(new,6-neighbours);
    new = new & low;
end
return new;
```

Fig. 1. Pseudo-algorithm for the hysteresis procedure

pseudo-code of the hysteresis procedure. In the experiments, we fixed the two thresholds to 5 and 0.9, respectively, based on some preliminary tests.

The resulting image after the last iteration is considered the final segmentation and is the output of the algorithm. This segmentation method that uses a combination of feature-space clustering and a hysteresis threshold will from now on be referred to as FCH.

2.6 Parameter Calculation

The final segmentations are used to calculate the following 7 different bone structure parameters:

1. Trabecular nodes (Tb.Nd) which is defined as the number of trabecular intersections per mm^3
2. Trabecular termini (Tb.Tm) which is defined as the number of free ends of trabeculae per mm^3
3. Trabecular separation (Tb.Sp) which is defined as the thickness of the spaces between the trabeculae in mm
4. Trabecular spacing (Tb.Sc) which is defined as the distance between the midlines of the trabeculae in mm
5. Trabecular number (Tb.N) which is defined as the number of trabeculae per mm
6. Trabecular thickness (Tb.Th) which is defined as the thickness of trabecular structures in mm
7. Bone volume over total volume (BV/TV) which is calculated by dividing the number of voxels defined as bone with the total number of voxels in the analysed volume.

All of the above parameters were calculated in 3D. Four parameters (Tb.Nd, Tb.Tm, Tb.Sc and Tb.N) were calculated after skeletonizing the binary image to one-voxel-wide lines using the method described in [22] without any pruning of the resulting skeleton.

Besides the above-mentioned structural parameters, the contrast to noise ratio (CNR) of the resulting segmentations were calculated and the time each segmentation method took to run was measured. In order to describe the agreement between different segmentation methods, the Dice coefficient was calculated, which is given by:

$$\mathrm{Dice}_{(S1,S2)} = \frac{2 \times |S1 \cap S2|}{|S1| + |S2|} \tag{3}$$

where S1 and S2 are two segmentations and $|.|$ is the number of voxels defined as bone by the segmentation.

The segmentation and calculation of the parameters were performed on a personal computer (PC) with an Intel Core i5-4460 (Intel Santa Clara, CA) at 3.2 GHz, 16 GB of random access memory (RAM) and a 64-bit system and was implemented in MATLAB.

2.7 Statistical Methods

Results from the calculation of the parameters are presented as mean values with standard deviations. The correlation coefficients that are presented are Pearson correlations with 95% confidence intervals. Statistics were calculated using MS Excel, the Dice coefficient was calculated in MATLAB, and all graphs and tables were created in MS Excel. Images were created in MATLAB and MeVisLab.

3 Experimental Results

The MSCT volumes were segmented using Otsu thresholding, our implementation of the ARG algorithm [11] and FCH. Our implementation of ARG has previously been used to segment HR-pQCT and CBCT trabecular volumes [7, 9, 13]. Micro-CT data were segmented using Otsu's threshold and used as a gold standard. Figure 2 shows the result of different segmentation for MSCT as well as raw-image slices for both MSCT and micro-CT.

Table 1 shows the mean and standard deviation of different histomorphometry parameters computed on the segmented images of both micro-CT and MSCT. As shown, all three segmentation methods used on the MSCT resulted in an underestimation of Tb.Nd and Tb.Tm by a factor of 65 to 140 and Tb.N was underestimated by a factor of about 2. Tb.Th and BV/TV were instead overestimated by a factor of about 4 and Tb.Sc was overestimated by a factor of approximately 2. Tb.Sp produced similar results for the micro-CT and MSCT data. Overall the three different segmentation methods used for the MSCT data produced results of similar magnitude.

Table 2 shows Pearson correlation coefficients for the different parameters using micro-CT as reference. All segmentation methods showed correlation coefficients of 0.70 or higher for all structure parameters except for Tb.Th where Otsu and FCH showed correlations approximately equal to 0 and ARG had a correlation coefficient of 0.61.

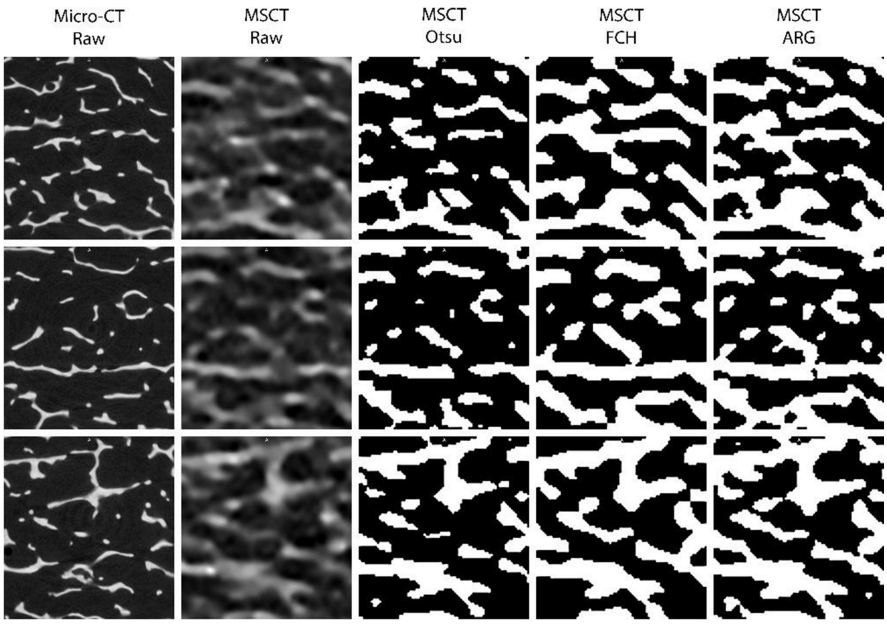

Fig. 2. Raw-image slices (left) for the micro-CT and the MSCT as well images from the MSCT segmented with the three different segmentation methods (right)

Table 1. Mean values of structural parameters, CNR and segmentation time in seconds ± standard deviations. *Tb.Nd* [mm^{-3}], *Tb.Tm* [mm^{-3}], *Tb.Sp* [mm], *Tb.Sc* [mm], *Tb.N* [mm^{-1}], *Tb.Th* [mm] and BV/TV [%]

Mean values ± SD										
		Tb.Nd	Tb.Tm	Tb.Sp	Tb.Sc	Tb.N	Tb.Th	BV/TV	CNR	Time
MSCT	Otsu	0.80 ± 0.22	0.67 ± 0.17	0.72 ± 0.09	1.23 ± 0.09	0.81 ± 0.06	0.46 ± 0.02	0.30 ± 0.08	5.15 ± 1.14	0.08 ± 0.02
	FCH	0.69 ± 0.16	0.61 ± 0.18	0.76 ± 0.10	1.40 ± 0.11	0.72 ± 0.06	0.58 ± 0.03	0.41 ± 0.10	4.74 ± 0.91	5.14 ± 1.36
	ARG	0.89 ± 0.16	0.75 ± 0.11	0.67 ± 0.06	1.20 ± 0.08	0.83 ± 0.05	0.48 ± 0.02	0.36 ± 0.07	5.68 ± 1.18	26.7 ± 8.16
micro-CT	Otsu	58.5 ± 15.6	86.3 ± 22.0	0.68 ± 0.10	0.74 ± 0.10	1.37 ± 0.18	0.13 ± 0.01	0.10 ± 0.03	29.4 ± 6.48	

Table 2. Correlation with micro-CT (reference method)

Pearson correlations coefficients (95% confidence interval)								
		Tb.Nd	Tb.Tm	Tb.Sp	Tb.Sc	Tb.N	Tb.Th	BV/TV
MSCT	Otsu	0.85 (0.58; 0.95)	0.80 (0.47; 0.93)	0.70 (0.27; 0.90)	0.76 (0.38; 0.92)	0.79 (0.45; 0.93)	−0.04 (−0.56; 0.50)	0.85 (0.58; 0.95)
	FCH	0.92 (0.76; 0.97)	0.87 (0.63; 0.96)	0.80 (0.47; 0.93)	0.90 (0.71; 0.97)	0.88 (0.66; 0.96)	−0.02 (−0.54; 0.52)	0.87 (0.63; 0.96)
	ARG	0.85 (0.58; 0.95)	0.77 (0.40; 0.92)	0.80 (0.47; 0.93)	0.89 (0.68; 0.96)	0.90 (0.71; 0.97)	0.61 (0.12; 0.86)	0.96 (0.88; 0.99)

FCH showed higher correlations than Otsu on all measured structural parameters with increases in correlation coefficients ranging from 0.02 for BV/TV to 0.14 for Tb.Sc. FCH also showed higher correlation than ARG when measuring Tb.Nd and Tb.Tm while having lower correlation when measuring BV/TV and Tb.Th. The average correlation for ARG was 0.08 higher than that of FCH when including Tb.Th whereas FCH was 0.01 higher when Tb.Th was excluded from the comparison.

The average segmentation times (Table 1) show that Otsu was about 64 times faster than FCH, which in turn was about 5 times faster than ARG.

The Dice coefficients for the segmentations on the MSCT data were 0.93 between ARG and Otsu, 0.82 between ARG and FCH and 0.80 between Otsu and FCH. These results show that ARG and Otsu produces more similar results compared to each than either compared to the proposed method.

4 Discussion

In this study we have investigated the potential use of MSCT data for measuring trabecular bone structure parameters as well as proposing a new method for segmenting trabecular bone.

The fact that a simple global threshold (like Otsu) might not work so well with clinical machines like the MSCT used in this study may be related to the low CNR, compared to micro-CT images, when imaging trabecular bone. One reason for the lower CNR and another possible reason why a global threshold performs poorly could be the partial volume effect where the large image voxels of the MSCT, and other clinical machines, only partly contains bone. This causes a lot of voxels with intermediary intensity values that are both bone and background.

The MSCT data showed relatively high correlation with the micro-CT data with correlations above 0.80 for all structure parameters except Tb.Tm and Tb.Th when using either the ARG or FCH algorithm. This suggest that it might be possible to use MSCT:s for measuring and monitoring trabecular bone structure.

Otsu was by far the quickest segmentation method with an average segmentation-time of 0.08 s, but it also had the lowest average correlation with micro-CT data. In contrast, the ARG algorithm had the highest average correlation coefficient and was the slowest algorithm with an average segmentation-time of 26.7 s. FCH showed higher correlations with micro-CT than Otsu for all parameters and, except for Tb.Th, it showed correlations similar to ARG while at the same time being significantly faster with an average segmentation time of 5.14 s.

As in previous studies from our group on clinical machines, the MSCT data underestimated Tb.Nd and Tb.N while overestimating Tb.Th and BV/TV [7, 9]. As an over- or underestimation in absolute values can be corrected if the correlation is high, a higher correlation is more relevant for detecting true differences between individuals.

The finding that the Otsu algorithm is the fastest of the three compared algorithms was expected, due to the simple calculations that are performed on the histogram of the data. As the ARG algorithm is an iterative algorithm and our implementation performs 50 iterations of the region growing with different homogeneity thresholds, it is reasonable for it to take longer than Otsu to segment the image. It is also reasonable that

FCH takes longer to segment the image than Otsu as it uses more computer-intensive calculations to segment the image. Clinical workflows are often time-pressed which means that if a new algorithm is to be widely accepted it needs to not only give accurate and valid results, it has to do so in as short a time as possible. This makes FCH an interesting contribution to the arsenal for analysing trabecular bone as it results in correlations similar to ARG while taking approximately one fifth as long to compute.

The low correlation for Tb.Th for both Otsu and FCH when compared to ARG is interesting and would be interesting to investigate further. There could be multiple reasons for this result, but so far no satisfactory explanation has been found. As a previous study from our group [7] has shown that Tb.Th has little to no impact on the overall strength of the trabecular network, as measured by FEM, a lower performance on this parameter might be acceptable although better performance of course is preferred.

One interesting result is the fact that the Dice coefficient for ARG-FCH (0.82) and Otsu-FCH (0.80) is so much lower than the Dice coefficient for ARG-Otsu (0.93). One explanation for this could be the fact that while they use different types of thresholds (homogeneity vs. intensity) and a different process for segmenting the image (region growing vs. a global threshold), both ARG and Otsu only use intensity data. FCH, on the other hand, also processes information based on edge detection, which could introduce another dimension to base the segmentation on and result in less similar segmentations. If one looks at the segmented slices in Fig. 2, both ARG and FCH seems to be preserving more of the structure of the trabecular bone, which could explain their higher correlations with the micro-CT data regarding trabecular bone structure parameters. The visual similarity, but low Dice coefficient, between ARG and FCH is something that warrants further investigation as it might help with further development of the algorithms

One of the weaknesses of this study is the fact that it only used 14 bones, which means that the statistical power is relatively low. One of the ongoing projects for our team is to include more bone specimens to verify our results in a bigger sample. It would also have been of interest to study the agreement of each of the segmentation methods applied to MSCT data to the micro-CT segmentation results using the Dice coefficient. However, registration problems between the modalities made this comparison impractical. Another of our ongoing projects is to test other clinical protocols with varying scanning parameters on the MSCT and a clinical trial to evaluate the performance of the CBCT used in [13] when measuring trabecular bone structure parameters in osteoporotic individuals.

In conclusion, the proposed segmentation method shows a reasonable balance between performance and computational intensity while the MSCT shows potential for analysing trabecular bone structure if the correct segmentation method is used.

References

1. Kleerekoper, M., Villanueva, A.R., Stanciu, J., Rao, D.S., Parfitt, A.M.: The role of three-dimensional trabecular microstructure in the pathogenesis of vertebral compression fractures. Calcif. Tissue Int. **37**(6), 594–597 (1985)
2. Ulrich, D., van Rietbergen, B., Laib, A., Ruegsegger, P.: The ability of three-dimensional structural indices to reflect mechanical aspects of trabecular bone. Bone **25**(1), 55–60 (1999)
3. Parkinson, I., Badiei, A., Stauber, M., Codrington, J., Müller, R., Fazzalari, N.: Vertebral body bone strength: the contribution of individual trabecular element morphology. Osteoporos. Int. **23**(7), 1957–1965 (2012)
4. Mosekilde, L.: Vertebral structure and strength. In vivo and in vitro. Calcif. Tissue Int. **53**, S121–S126 (1993)
5. Thomsen, J.S., Laib, A., Koller, B., Prohaska, S., Mosekilde, L., Gowin, W.: Stereological measures of trabecular bone structure: comparison of 3D micro computed tomography with 2D histological sections in human proximal tibial bone biopsies. J. Microsc. **218**(Pt 2), 171–179 (2005)
6. Burghardt, A.J., Pialat, J.B., Kazakia, G.J., Boutroy, S., Engelke, K., Patsch, J.M., et al.: Multicenter precision of cortical and trabecular bone quality measures assessed by high-resolution peripheral quantitative computed tomography. J. Bone Mineral Res.: Official J Am. Soc. Bone Mineral Res. **28**(3), 524–536 (2013)
7. Klintström, E., Klintström, B., Moreno, R., Brismar, T.B., Pahr, D.H., Smedby, Ö.: Predicting trabecular bone stiffness from clinical cone-beam CT and HR-pQCT data; An in vitro study using finite element analysis. PLoS ONE **11**(8), e0161101 (2016)
8. Bauer, J.S., Link, T.M., Burghardt, A., Henning, T.D., Mueller, D., Majumdar, S., et al.: Analysis of trabecular bone structure with multidetector spiral computed tomography in a simulated soft-tissue environment. Calcif. Tissue Int. **80**(6), 366–373 (2007)
9. Klintström, E., Smedby, Ö., Moreno, R., Brismar, T.B.: Trabecular bone structure parameters from 3D image processing of clinical multi-slice and cone-beam computed tomography data. Skeletal Radiol. **43**(2), 197–204 (2014)
10. Bouxsein, M.L., Boyd, S.K., Christiansen, B.A., Guldberg, R.E., Jepsen, K.J., Muller, R.: Guidelines for assessment of bone microstructure in rodents using micro-computed tomography. J. Bone Mineral Res.: Official J. Am. Soc. Bone Mineral Res. **25**(7), 1468–1486 (2010)
11. Revol-Muller, C., Peyrin, F., Carrillon, Y., Odet, C.: Automated 3D region growing algorithm based on an assessment function. Pattern Recogn. Lett. **23**(1–3), 137–150 (2002)
12. Kettaf, F., Bi, D., de Beauville, J.A.: A comparison study of image segmentation by clustering techniques. In: 3rd International Conference on Signal Processing. IEEE (1996)
13. Klintström, E., Smedby, Ö., Klintström, B., Brismar, T.B., Moreno, R.: Trabecular bone histomorphometric measurements and contrast-to-noise ratio in CBCT. Dentomaxillofacial Radiol. **43**(8), 20140196 (2014)
14. Petersson, J., Brismar, T., Smedby, Ö.: Analysis of skeletal microstructure with clinical multislice CT. In: Larsen, R., Nielsen, M., Sporring, J. (eds.) MICCAI 2006. LNCS, vol. 4191, pp. 880–887. Springer, Heidelberg (2006). doi:10.1007/11866763_108
15. Moreno, R., Borga, M., Klintström, E., Brismar, T., Smedby, Ö.: Anisotropy estimation of trabecular bone in gray-scale: comparison between cone beam and micro computed tomography data. In: Tavares, J.M.R.S., Jorge, R.N. (eds.) Developments in Medical Image Processing and Computational Vision. LNCVB, vol. 19, pp. 207–220. Springer, Cham (2015). doi:10.1007/978-3-319-13407-9

16. Moreno, R., Borga, M., Klintström, E., Brismar, T., Smedby, Ö.: Correlations between fabric tensors computed on cone beam and micro computed tomography images. In: Computational Vision and Medical Image Processing (VIPIMAGE), pp. 393–398. CRC Press (2013)
17. Otsu, N.: Threshold selection method from gray-level histograms. IEEE Trans. Syst. Man Cybern. **9**(1), 62–66 (1979)
18. Hartigan, J.A.: Clustering algorithms (1975)
19. Hartigan, J.A., Wong, M.A.: Algorithm AS 136: a k-means clustering algorithm. J. Roy. Stat. Soc.: Ser. C (Appl. Stat.) **28**(1), 100–108 (1979)
20. Canny, J.: A computational approach to edge detection. IEEE Trans. Pattern Anal. Mach. Intell. **8**(6), 679–698 (1986)
21. Sobel, I., Feldman, G.: A 3 × 3 isotropic gradient operator for image processing. A talk at the Stanford Artificial Project. pp. 271–272 (1968)
22. Xie, W., Thompson, R.P., Perucchio, R.: A topology-preserving parallel 3D thinning algorithm for extracting the curve skeleton. Pattern Recogn. **36**(7), 1529–1544 (2003)